Monthly Notices
of the
ROYAL ASTRONOMICAL SOCIETY

MNRAS **487,** 1994–2004 (2019)
Advance Access publication 2019 May 17

doi:10.1093/mnras/stz1372

Constraints on magnetospheric radio emission from Y dwarfs

Melodie M. Kao,[1,2]★† Gregg Hallinan[1] and J. Sebastian Pineda[3]

[1]*California Institute of Technology, Department of Astronomy, 1200 E California Blvd, MC 249-17, Pasadena CA 91125, USA*
[2]*School of Earth and Space Exploration, Arizona State University, 550 E Tyler Mall, PSF 686, Tempe AZ 85287, USA*
[3]*Laboratory for Atmospheric and Space Physics, University of Colorado Boulder, 3665 Discovery Drive, Boulder CO 80303, USA*

Accepted 2019 May 6. Received 2019 May 6; in original form 2019 January 1

ABSTRACT

As a pilot study of magnetism in Y dwarfs, we have observed the three known infrared variable Y dwarfs *WISE* J085510.83−071442.5, *WISE* J140518.40+553421.4, and *WISEP* J173835.53+273258.9 with the NSF's Karl G. Jansky Very Large Array in the 4–8 GHz frequency range. The aim was to investigate the presence of non-bursting quiescent radio emission as a proxy for highly circularly polarized radio emission associated with large-scale auroral currents. Measurements of magnetic fields on Y dwarfs may be possible by observing auroral radio emission, and such measurements are essential for constraining fully convective magnetic dynamo models. We do not detect any pulsed or quiescent radio emission, down to rms noise levels of 7.2 μJy for *WISE* J085510.83−071442.5, 2.2 μJy for *WISE* J140518.40+553421.4, and 3.2 μJy for *WISEP* J173835.53+273258.9. The fractional detection rate of radio emission from T dwarfs is ∼10 per cent suggesting that a much larger sample of deep observations of Y dwarfs is needed to rule out radio emission in the Y dwarf population. We discuss a framework that uses an empirical relationship between the auroral tracer Hα emission and quiescent radio emission to identify brown-dwarf auroral candidates. Finally, we discuss the implications that Y dwarf radio detections and non-detections can have for developing a picture of brown dwarf magnetism and auroral activity.

Key words: planets and satellites: aurorae – planets and satellites: magnetic fields – brown dwarfs – stars: individual: *WISE* J085510.83−071442.5 – stars: individual: *WISE* J140518.40+553421.4 – stars: individual: *WISEP* J173835.53+273258.9.

1 INTRODUCTION

Y dwarfs are the most newly discovered brown dwarf spectral class with effective temperatures approaching planetary values at only ∼350 K. They are the current frontier of brown dwarf science and its synergistic relationship with exoplanet and planetary science. One vital stepping stone that they may provide is mapping out how magnetism evolves from brown dwarfs to planets.

An important outstanding problem in dynamo theory is understanding how magnetic fields are generated and sustained in fully convective objects, spanning both stars and planets. Whereas prevailing dynamo models for dwarf stars with an inner radiative zone and an outer convective envelope rely on the strong differential rotation at the interface between the two layers to power $\alpha\Omega$ dynamos (Parker 1975), fully convective dwarfs do not support such a dynamo. Despite this they exhibit tracers of magnetic activity such as Hα emission (Gizis et al. 2000; Reiners & Basri 2008; West et al. 2008; Schmidt et al. 2015; Miles-Páez et al. 2017) and radio emission (Berger et al. 2001; Berger 2002; Burgasser & Putman 2005; Berger 2006; Hallinan et al. 2006, 2007, 2008; Antonova et al. 2007; Phan-Bao et al. 2007; McLean et al. 2011; McLean, Berger & Reiners 2012; Burgasser et al. 2013; Williams, Cook & Berger 2014; Burgasser et al. 2015; Williams & Berger 2015; Kao et al. 2016, 2018; Route & Wolszczan 2016a; Williams, Gizis & Berger 2017;) down to spectral type T6.5. In fact, Zeeman broadening and Zeeman Doppler imaging studies confirm surface-averaged magnetic field magnitudes of order kilogauss on dwarfs as late as M9 (Saar 1994; Johns-Krull & Valenti 1996; Donati et al. 2006; Reiners & Basri 2007, 2009, 2010; Morin et al. 2010; Shulyak et al. 2017), and pulsed radio emission associated with ∼kG fields has been observed on objects as late as T6.5 (Route & Wolszczan 2012; Kao et al. 2016; Route & Wolszczan 2016a). Instead of the $\alpha\Omega$ dynamo, these fully convective objects must rely on alternate dynamo mechanisms to support such fields.

A number of models for possible dynamo mechanisms in this regime have been proposed (e.g. Browning 2008; Christensen, Holzwarth & Reiners 2009; Simitev & Busse 2009; Morin et al. 2011; Gastine et al. 2013), but constraining data on magnetic field

★ E-mail: mkao@asu.edu
† NASA Hubble Fellow.

strengths and topologies across a wide range of mass, age, rotation rate, and temperature are sorely lacking, particularly in the brown dwarf regime. L, T, and Y dwarfs probe the lowest end of the substellar mass and temperature space – a regime that is necessary for validating and constraining any fully convective dynamo model.

One notable dynamo scaling relation predicts that convected energy flux sets magnetic energy in fully convective stars through planets (Christensen et al. 2009) and is derived from a suite of dynamo simulations using a model described in Christensen and Aubert (2006). It predicts considerably weaker magnetic fields for Y dwarfs at ∼hundreds of gauss compared to ∼kilogauss fields on L and T dwarfs and a few kilogauss fields for M dwarfs. Any ∼kilogauss Y dwarf measurement unequivocally challenges this model. In this light, even a single Y dwarf magnetic field measurement at 4–8 GHz (corresponding to 1.4–2.9 kG fields) would be significant and support emerging evidence suggesting that mid-M, through late L and T dwarfs, can produce surface-averaged magnetic fields that are systematically stronger than leading predictions (Shulyak et al. 2017; Kao et al. 2018).

Traditional techniques that rely on Zeeman broadening have successfully measured the strength, filling factor, and large-scale field topologies of objects as late as M9 (Johns-Krull & Valenti 1996; Donati et al. 2006; Reiners & Basri 2006, 2007; Morin et al. 2010; Shulyak et al. 2017). However, unresolved Zeeman splitting components require careful modelling and measurements of lines with very low Landé factors to distinguish Zeeman broadening from other sources, such as thermal, collisional, and rotational broadening (Valenti, Marcy & Basri 1995).

Reiners & Basri (2007) were able to measure mean magnetic field magnitudes by comparing the FeH features of 24 M2–M9 stars to reference spectra with known mean surface field magnitudes, with ∼15–30 per cent uncertainties (Shulyak et al. 2010; Reiners 2012). The method described by Reiners & Basri (2006) is limited by the reference spectra: mean magnetic field magnitudes are measured in reference to a zero field spectrum and a 3.9 kG spectrum. Using these reference spectra, only fields less than 3.9 kG can be quantified, though it is unlikely that the object serving as the zero field reference is in fact magnetically inactive. By comparing models of synthetic spectra to observed spectra and targeting Ti I lines with known Landé factors, Shulyak et al. (2017) were able to measure magnetic fields as strong as ∼7.5 kG. These new detections may be able to extend the Reiners & Basri (2006) techniques to similar magnetic field strengths. However, Zeeman broadening techniques have yet to be successfully applied to objects beyond M9, where rotational broadening blends known useful molecular lines and FeH and Ti lines saturate. Detailed theoretical treatments remain limited for determining the values of Landé factors and therefore the magnetic sensitivity of a given line (Berdyugina & Solanki 2002; Shulyak et al. 2010), preventing these techniques from accessing L and later dwarfs.

Detections of highly circularly polarized and pulsed radio emission currently provide our only window into magnetic field measurements for L and T dwarfs, and may do the same for Y dwarfs. This emission is attributed to the electron cyclotron maser (ECM) instability (Hallinan et al. 2008), which is also responsible for producing the auroral radio emission from all of the magnetized planets in our Solar system (Zarka 2007). Auroral magnetic activity is distinct from the standard stellar chromospheric heating picture, where magnetic fields locally interact with hotter and less neutral atmospheres to drive transient, small-scale currents, such as magnetic reconnection events and coronal loops. Instead, brown dwarf magnetic activity or a component of it may be more analogous to what has been observed in Jupiter. In the planetary case, tracers of magnetic activity such as optical, infrared, and UV aurora (Bhardwaj & Gladstone 2000; Clarke et al. 2004; Grodent et al. 2009; Maillard & Miller 2011; Dyudina et al. 2016; Moore et al. 2017) are powered by an external source, the outer magnetosphere, via auroral current systems, such as magnetosphere–ionosphere coupling currents that give rise to auroral activity (Schrijver 2009; Nichols et al. 2012; Bagenal et al. 2014; Turnpenney et al. 2017).

ECM emission is a powerful tool for measuring magnetic fields, and it has provided some of the first confirmations of kilogauss fields for late M and L dwarfs (Burgasser & Putman 2005; Hallinan et al. 2006, 2007, 2008; Berger et al. 2009). Mutel et al. (2006) show that high-ECM growth rates occur when

$$\frac{f_{\rm pe}(n_e)}{f_{\rm ce}} < \left[\frac{\gamma - 1}{\gamma}\right]^{1/2}, \quad (1)$$

where $f_{\rm pe}$ is the electron plasma frequency, $f_{\rm ce}$ is the electron cyclotron frequency, γ is the Lorentz factor, and n_e is the electron density. For an ultrarelativistic electron population where $\gamma \gg 1$, significant ECM growth rates can occur at high densities $n_e < 10^{11} \times B_{\rm kilogauss}$ cm^{-3} (Lynch, Mutel & Güdel 2015). For mildly relativistic electron populations, the density condition becomes $n_e < 1.24 \times 10^{10} f_{\rm GHz}^2$ (Treumann 2006) and favours low-plasma densities where $f_{pe}^2/f_{ce}^2 \ll 1$. When the ratio of the plasma frequency to the electron cyclotron frequency exceeds ∼0.3, emission at the second and higher harmonics can dominate, whereas the fundamental frequency is expected to dominate at low densities (Winglee 1985).

Y dwarfs were only recently discovered (Cushing et al. 2011), and little is currently empirically known about Y dwarf magnetism and magnetic activity. Instead, we can extrapolate from the magnetic behaviours of their slightly warmer L and T dwarf cousins and their gas giant planetary counterparts. Models of local plasma densities in the neutral atmospheres of late L and T dwarfs (Rodriguez-Barrera et al. 2015) imply that observed ECM emission in these cold brown dwarfs will be dominated by the fundamental frequency for the frequencies typically observed (a few GHz). Extrapolating plasma density models to the effective temperatures of Y dwarfs (∼350 K) suggests the same for these coldest and most planet-like brown dwarfs. Similarly, the sharp drop in X-ray luminosities observed in late M dwarfs (e.g. Williams et al. 2014; Pineda, Hallinan & Kao 2017) indicate that as the atmospheres of ultracool dwarfs and brown dwarfs become cooler, magnetic fields are less able to couple to the consequently more neutral atmospheres (Mohanty et al. 2002), beginning at effective temperatures that can be nearly an order of magnitude higher than those of Y dwarfs.

Observations of the Solar system planets, with atmospheric temperatures up to ∼300 K, confirm emission at almost exactly the fundamental electron cyclotron frequency $\nu_{\rm MHz} \sim 2.8 \times B_{\rm Gauss}$ (and references therein, Treumann 2006). ECM emission frequencies in the coolest brown dwarfs likely, also uniquely and accurately, identify the local magnetic field strengths in the regions of the magnetosphere from where the emission originates. Near the surface of the atmosphere, where the magnetic field is the strongest and produces the highest frequency emission, conditions necessary for generating observable ECM emission cease to occur, causing a sharp drop-off in the emission (Zarka 1998). This high-frequency ECM emission cut-off corresponds to the lower bound of the maximum large-scale magnetic field strengths in the coolest substellar objects (Kao et al. 2016).

Radio detections of brown dwarfs are rare. Radio surveys encompassing objects later than M7 have yielded a ∼10 per cent

detection rate (Berger 2006; Lynch et al. 2016; Route & Wolszczan 2016b), and until 2016, only one detection out of ∼60 L6 or later targets (Antonova et al. 2013; Route & Wolszczan 2013). In a previous study, we developed a selection strategy for biasing survey targets based on possible optical and infrared tracers of auroral activity (Kao et al. 2016). Our selection process was motivated by (a) low-amplitude *I*-band variability detected in known auroral radio emitters (Harding et al. 2013); (b) simultaneous radio and optical spectroscopic observations of an M8.5 dwarf showing Balmer line and optical broad-band continuum variability tracking auroral radio pulses (Hallinan et al. 2015); and (c) predictions of increased emission at *K*-band or longer wavelengths from localized atmospheric heating (e.g. an impacting auroral current; Morley et al. 2014).

Using our selection strategy, we detected highly circularly polarized radio emission for four of five pilot targets at 4–8 GHz, confirming >2.5 kG magnetic fields. By carefully comparing the magnetic field measurements derived from radio emission to lower bound measurements that would have been derived from Zeeman broadening and Zeeman Doppler imaging for the same field, we provided tentative evidence that the dynamo operating in this mass regime may be inconsistent with predicted values from Christensen et al. (2009). This suggested that parameters beyond convective flux may influence magnetic field generation in brown dwarfs.

To access the strongest constraints on fully convective dynamo models, pushing magnetic field measurements to Y dwarfs and eventually exoplanets, such as hot Jupiters, is critical. While previous searches for radio emission from exoplanets have been attempted, the work presented here is the first such attempt for Y dwarfs and is motivated by the success of our above described selection strategy and recent discoveries of variability at near- and/or mid-infrared bands for three Y dwarfs, *WISE* J140518.39+553421.3, *WISE* J085510.83−071442.5, and *WISEP* J173835.52+273258.9 (Cushing et al. 2016; Esplin et al. 2016; Leggett et al. 2016). These detections of variability have been quite reasonably attributed to variations in atmospheric temperature or opacity (weather), but it has been argued that similar phenomena can be driven by auroral currents for the ∼10 per cent of objects that exhibit radio pulsing (Hallinan et al. 2015; Kao et al. 2016; Pineda et al. 2017).

If so, observational evidence demonstrates that aurora may play a role in some cloud variability cases, but not all. The radio fractional detection rates are low (Route & Wolszczan 2016b) compared to cloud phenomena, where up to ∼80 per cent of L or T transition brown dwarfs may be strong variables (>2 per cent peak-to-peak amplitudes), and ∼60 per cent of L and T dwarfs outside of spectral types L9–T3.5 may be more moderate variables (0.5–1.6 per cent peak-to-peak amplitudes) at *J*- and *K*-bands (Radigan et al. 2014). Similarly, 3–5 μm variability may be ubiquitous for L and T dwarfs (Metchev et al. 2015), yet infrared variability is not correlated with another tracer of aurora, Hα emission (Miles-Páez et al. 2017).

In exoplanets, the primary driver of auroral emission is expected to be the interaction of the planetary magnetosphere with the stellar wind, and emission intensities therefore depend strongly on incident stellar wind flux (Gallagher & Dangelo 1981; Gurnett et al. 2002). Attempts to detect hot Jupiter radio emission have thus far been unsuccessful (e.g. Hallinan et al. 2013; Murphy et al. 2015; Bower et al. 2016; Lynch et al. 2017).

In isolated brown dwarfs likely drivers for auroral emission include the co-rotation breakdown of a plasma sheet in the brown dwarf magnetosphere (Cowley & Bunce 2001; Hill 2001) or the current generated by the relative motion of a planetary satellite with respect to the brown dwarf magnetosphere (Zarka 2007). As such, radio power from isolated brown dwarfs is not limited by incident stellar wind flux but instead depends on plasma conditions and the voltage drop generated across auroral current systems driven by large-scale magnetic fields (Nichols et al. 2012; Turnpenney et al. 2017). If the generation of strong large-scale magnetic fields is indeed dependent on convected energy (i.e. temperature) as suggested by Christensen et al. (2009), Y dwarf radio detection fractions may be unlikely to depart precipitously from reported ∼5–10 per cent detection fractions (Route & Wolszczan 2016b; Pineda et al. 2017; Route 2017), as brown dwarfs spend their lifetimes gravitationally contracting and cooling along the L–T–Y spectral sequence.

We present here an initial pilot study of three nearby exemplar Y dwarfs with evidence of IR variability.

2 TARGETS

For our study, we observed the three known IR-variable Y dwarfs. Our selection strategy is motivated by the success of our previous survey in which we newly detected both pulsed and quiescent radio emission in 4 or 5 late L and T dwarfs by selecting for tracers of auroral emission at other wavelengths (Kao et al. 2016), specifically Hα and infrared variability. Although none of the targeted Y dwarfs have confirmed Hα emission, their IR variability is similar in nature to that of SIMP J01365662+0933473 (hereafter SIMP0136), a T2.5 dwarf known to emit auroral ECM pulses at 4–8 GHz. SIMP0136 was the first clearly periodic and high-amplitude IR variable T dwarf, yet it lacks detectable Hα emission (Pineda et al. 2017). Clouds in brown dwarf atmospheres have been proposed to interpret observed photometric and spectroscopic variability (Marley, Saumon & Goldblatt 2010; Apai et al. 2013; Burgasser et al. 2014), but the Kao et al. (2016) results point to the possibility that an additional variability mechanism may be at play in some cases, e.g. extreme variables like SIMP0136, as postulated by Hallinan et al. (2015). We stress that brown dwarf weather is much more prevalent than radio emission (Radigan et al. 2014; Pineda 2016; Route 2016), and Hα emission and photometric variability are not correlated in L0–T8 dwarfs (Miles-Páez et al. 2017), so at least some fraction of that variability is likely causally unrelated. Target properties are listed in Table 1.

***WISE* J085510.83−071442.5**. *WISE* 0855−07 was identified as a high-proper motion object in the *Wide-field Infrared Survey Explorer* (*WISE*) catalogue (Wright et al. 2010) by Luhman (2014), with a parallax corresponding to ∼2.2 pc. The authors estimated that 225 K < $T_{\rm eff}$ < 260 K, and noting that it was the reddest known T or Y dwarf, tentatively identified it as a Y dwarf. In a follow-up study, Faherty et al. (2014) confirmed 225 K < $T_{\rm eff}$ < 250 K, and a tentative *J*3 detection provided evidence that *WISE* 0855−07 may host sulphide and water ice clouds. The presence of atmospheric water vapour and clouds was confirmed by a 4.5–5.2 μm spectrum obtained by Skemer et al. (2016). In contrast, Luhman & Esplin (2016) were unable to conclusively constrain the presence of clouds or non-equilibrium chemistry in its atmosphere when comparing photometry in six optical and near-IR bands to model predictions. Finally, Esplin et al. (2016) reported variability at 3.6 μm and 4.5 μm with peak-to-peak amplitudes between 3–5 per cent and also found insufficient evidence for water ice clouds in the atmosphere. Periodicity in the observed variability was inconclusive, with periods ranging between 6.8–9.0 h at 3.6 μm and 5.3–9.3 h at 4.5 μm for two different epochs.

***WISE* J140518.40+553421.4**. *WISE* 1405+55 was discovered and initially classified as a Y0p? dwarf by Cushing et al. (2011),

Table 1. Target properties.

Object name	Abbrev. name	SpT	Parallax (mas)	Distance (pc)	$\mu_\alpha \cos\delta$ (mas yr^{-1})	μ_δ (mas yr^{-1})	Var. period (h [3.6],[4.5])	Ref.
WISE J085510.83−071442.5	*WISE* 0855−07	Y	449 ± 8	2.23 ± 0.04	−8118 ± 8	−680 ± 7	6.8/9.3, 9.0/5.3[a]	1–3
WISE J140518.40+553421.4	*WISE* 1405+55	Y0.5p?[b]	129 ± 19	$7.8^{+1.3}_{-1.0}$	−2263 ± 47	−288 ± 41	8.2 ± 0.3 / 8.54 ± 0.08[c]	4–7
*WISE*P J173835.53+273258.9	*WISE* 1738+27	Y0	128 ± 10	7.8 ± 0.6	−317 ± 9	−321 ± 11	6.0 ± 0.1[d]	5 8 9

[a]Esplin et al. (2016) report the listed Lomb–Scargle periodogram peaks for 3.6 μm or 4.5 μm, respectively, for two different epochs. They also report that a double sinusoid model in which one period is twice that of the other returns $9.7^{+0.9}_{-0.8}/10.8^{+0.7}_{-0.7}$ for 3.6 μm or 4.5 μm, respectively, the first epoch and $14^{+2}_{-2}/13.3^{+0.5}_{-0.4}$ for the second epoch.
[b]Cushing et al. (2016) identified that the p? had been mistakenly dropped by Schneider et al. (2015).
[c]Reported variability periods are for 3.6 μm and 4.5 μm, respectively.
[d]Leggett et al. (2016) report that the 4.5 μm variability can be fit with a double sinusoid with periods of 6.0 ± 0.1 h and 3.0 ± 0.1 h. They interpret this as evidence for a 6.0 ± 0.1 h rotation period with one or more sources of variability on the surface of *WISE* 1738+27.
References – (1) Luhman (2014); (2) Luhman & Esplin (2016); (3) Esplin et al. (2016) (4) Cushing et al. (2016); (5) Dupuy & Kraus (2013); (6) Cushing et al. (2011); (7) Kirkpatrick et al. (2011); (8) Beichman et al. (2014); (9) Leggett et al. (2016)

who noted that its *H*-band peak was ∼60 Å redder than the Y0 spectral standard. They estimated $T_{\rm eff}$ ∼350 K, log g ∼5.00, and M ∼30 $M_{\rm J}$. *Hubble Space Telescope (HST)* spectroscopy by Schneider et al. (2015) reclassified it as Y0.5, and confirmed that 350 K < $T_{\rm eff}$ < 400 K, and 5.0 < log g < 5.5. Parallax measurements confirm a distance of $7.8^{+1.3}_{-1.0}$ pc (Dupuy & Kraus 2013). *WISE* 1405+55 is the first Y dwarf from which photometric variability was detected at 3.6 μm and 4.5 μm with semi-amplitudes of 3.5 per cent and a period of ∼8.5 h (Cushing et al. 2016). The authors reported that current cloud and hot-spot models cannot reproduce the observed variability.

***WISEP* J173835.53+273258.9**. *WISE* 1738+27 was discovered by Cushing et al. (2011) and classified as a Y0 dwarf with an effective temperature of 430^{+50}_{-40} K (Dupuy & Kraus 2013), and it serves as the Y0 spectral standard (Kirkpatrick et al. 2012). Its parallax of 128 ± 10 mas corresponds to a distance of 7.8 ± 0.6 pc (Beichman et al. 2014). Rajan et al. (2015) previously reported that it exhibited no statistically significant *J*-band variability, though they were only able to place an upper limit of <20.3 per cent on the amplitude. In contrast, Leggett et al. (2016) observed 4.5 μm variability characteristic of a double sinusoid with 6.0 ± 0.1 h and 3.0 ± 0.1 h periods and peak-to-peak amplitude 3 per cent, whereas near-infrared monitoring at 1 μm and *Y*- and *J*-bands are marginally consistent with a ∼3.0 h period and amplitudes as high as ∼5–30 per cent. The wavelength dependence and amplitude of the variability suggests atmospheric phenomena similar to what has been observed in the Solar system gas giant planets.

3 OBSERVATIONS

We observed the three Y dwarfs with the full VLA array in *C*-band (4–8 GHz), using the WIDAR correlator in 3-bit observing mode for 4 GHz bandwidth observations. *WISE* 0855−07 and *WISE* 1405+55 comprised our initial pilot study with time blocks of 4 h each on 2015 May 22 and 2015 May 16, respectively, during BnA configuration. *WISE* 1738+27 was included as a later target in a separate study, and we observed it for 2 h on 2016 April 06 during C configuration. We summarize target observations in Table 2.

Searching for rotationally modulated auroral pulses can be time intensive, requiring more than one full rotation period to observe at least two pulses. Due to the longer rotational periods for our targets, we elected to search for quiescent (non-bursting) radio emission as a proxy for pulsed emission, with the aim to follow up any quiescent detections for pulsed emission at a later date.

Targeting quiescent emission brings additional advantages. While Jovian auroral emission cuts off at ∼40 MHz (14 Gauss), its quiescent emission is broad-band from a few MHz up to a few GHz (Zarka 2007). Likewise, auroral ultracool dwarfs and brown dwarfs are known to emit pulses at $\gtrsim$4–15 GHz (Hallinan et al. 2006, 2007, 2008, 2015; Route & Wolszczan 2012, 2013; Williams & Berger 2015; Lynch et al. 2015; Kao et al. 2016, 2018; Route 2016; Williams et al. 2017) and quiescent emission up through 95 GHz (Williams et al. 2015; Kao et al. 2016, 2018; Lynch et al. 2016). As intermediaries between gas giant planets and T dwarfs, Y dwarfs that emit pulsed and/or quiescent emission likely do so in the frequency ranges spanning planetary and ultracool dwarfs for the respective types of emission. Further informing our 4–8 GHz observing frequencies is the possibility that Y dwarfs may host the kilogauss fields probed at *C*-band, and observing at those frequencies may lead to a serendipitous detection of an ECM pulse. Even if their magnetic fields are weaker than the 1.4 kG field implied by 4 GHz ECM emission, quiescent synchrotron or gyrosynchrotron emission can occur at many multiples of the cyclotron frequency of the local magnetic field. Finally, observations spanning 10 yr confirmed that the quiescent emission can be temporally stable (e.g. Hallinan et al. 2006; Gawroński, Goździewski & Katarzyński 2017), though we note two exceptions in the existing literature where the L2.5 dwarf 2MASS J05233822−1403022 (Berger 2006; Antonova et al. 2007; Berger et al. 2010) and the M9.5 dwarf BRI 0021 (Berger et al. 2010) show long term variability in the quiescent emission at *C*-band frequencies.

3.1 An empirical connection between auroral emission and quiescent radio emission

Our choice to target quiescent (non-bursting) emission is motivated by the fact that detections of quiescent radio emission at 4–8 GHz have accompanied all previous auroral pulse detections (Burgasser & Putman 2005; Hallinan et al. 2007, 2008; Berger et al. 2009; Kao et al. 2016) or been discovered when pulsing dwarfs detected by Arecibo (which is insensitive to quiescent emission) were followed up with the VLA (Route & Wolszczan 2012; Williams, Berger & Zauderer 2013; Route & Wolszczan 2016a; Williams et al. 2017).

The actual mechanism for brown dwarf quiescent radio emission remains unconfirmed. However, the radio emissions of Solar system planets can give us some insight into possible quiescent radio mechanisms. Jovian radio emission has three main sources: (1) bursting ECM emission from electrons accelerated to keV energies at tens of

Table 2. Summary of observations.

Object	Band[a] (GHz)	Obs. date	Obs. block (h)	Time on source (s)	VLA configuration	Synthesized beam dimensions (arcsec × arcsec)	I, V RMS (μJy)	Phase calibrator	Flux calibrator
WISE 0855−07	4.0–8.0	2015 May 22	4.0	11862	BnA	1.37 × 0.73	7.2, 2.4	J0902−1415	3C286
WISE 1405+55	4.0–8.0	2015 May 16	4.0	12360	BnA	1.38 × 1.21	2.2, 2.3	J1419+5423	3C295[b]
WISE 1738+27	4.0–8.0	2016 Apr 06	2.0	5368	C	4.04 × 3.61	3.2, 2.9	J1753+2848	3C286

[a]All 4.0–4.4 GHz data was flagged for RFI.
[b]3C295 was fully resolved and unsuitable for flux calibrations. Instead, we transferred flux calibrations using 3C286 of an archival measurement set containing observations of our phase calibrator.

planetary radii that precipitate along magnetic field lines to produce ∼100 per cent circularly polarized and pulsing radio aurorae at frequencies corresponding to the local cyclotron frequency, up to ∼40 MHz for ∼14 Gauss fields (Zarka 1998; Clarke et al. 2004); (2) quiescent broad-band synchrotron radiation with ∼20–30 per cent linear polarization from high-energy electrons trapped in radiation belts within ∼10 R_J of its surface at frequencies overlapping ECM frequencies and extending up to hundreds of multiples of the local cyclotron frequency, or ∼14 GHz for Jupiter (Bolton et al. 2004; Khurana et al. 2004; Girard et al. 2016); and (3) quiescent thermal emission from the planetary disc, which dominates at high frequencies or above ∼4 GHz for Jupiter (Kloosterman, Butler & de Pater 2008; de Pater et al. 2016). In addition to Jupiter, the remaining strongly magnetized Solar system planets (Earth, Saturn, Uranus, and Neptune) produce radio emission from the above-described three main sources (Kellermann 1970; Basharinov, Gurvich & Egorov 1974; Mauk & Fox 2010; Ganushkina et al. 2011)

Here we focus on radiation belts as a possible source of quiescent radio emission since their emission dominates thermal emission at frequencies that are within a factor of ∼100 of the local cyclotron frequency, as is likely the case for our observations of Y dwarfs. The energetic particles in the radiation belts are trapped in regions extending up to 3.5–18 planetary radii (Stone & Miner 1986; Cruikshank, Matthews & Schumann 1995; Khurana et al. 2004; Walt 2005; André et al. 2008). The large-scale components of the planetary magnetic fields populate the planetary radiation belts by capturing energetic particles from sources including the solar wind, flares, and coronal mass ejections (Brice & Mcdonough 1973; Stansberry & White 1974; Hudson et al. 2004, 2008; Khurana et al. 2004), and volcanic moons such as Io (Khurana et al. 2004). In Jupiter, radiation belt electrons are accelerated to tens of keV up through tens of MeV (Bolton et al. 2004) via processes that transfer planetary rotational energy (Horne et al. 2008). These same processes may occur in the magnetospheres of isolated brown dwarfs, though the possibility has not yet been investigated.

Jupiter's intense radiation belts form as a consequence of the large source of plasma provided by Io. Io also provides the electron reservoir for the main oval of the Jovian aurora (Clarke et al. 2004) and demonstrates how quiescent radio emission and ECM radio aurora can be linked. Io is the dominant source of plasma in the Jovian magnetosphere, and the iogenic plasma is cooler and denser than the hot, diffuse plasma in its outer magnetosphere. As the iogenic plasma diffuses outward, the hot outer magnetosphere plasma diffuses inward, eventually resulting in radiation belts that extend out to 10 R_J (Horne et al. 2008). Meanwhile, iogenic plasma that has escaped outwards to Jupiter's middle and outer magnetosphere between $\gtrsim$20−40 R_J eventually ceases to co-rotate with Jupiter (Clarke et al. 2004; Khurana et al. 2004), generating strong field-aligned currents (Cowley & Bunce 2001). These strong currents precipitate the electrons into the upper atmosphere of Jupiter at high latitudes, emitting electron cyclotron maser emission from these mildly relativistic electrons and causing its main auroral ovals (Cowley & Bunce 2001). Such currents may also explain the ECM emission observed in isolated brown dwarfs (Schrijver 2009; Nichols et al. 2012; Turnpenney et al. 2017).

The existence of radiation belts in brown dwarf magnetospheres remains unconfirmed, but stable quiescent emission with circular polarization up to several tens of per cent (Williams & Berger 2015; Kao et al. 2016, 2018) point to trapped populations of mildly relativistic electrons in brown dwarf magnetospheres. A detection of 95 GHz quiescent emission from the M9 dwarf TVLM 513−46546, a known radio aurora source, suggests that a gyrosynchrotron emission process is occurring within its magnetosphere (Williams & Berger 2015), possibly from a radiation belt composed of particles with a lower energy distribution than in the Jovian belts. Terrestrial planets around brown dwarfs are predicted (He, Triaud & Gillon 2017), providing possible plasma sources for brown dwarf radiation belts. Further observations and modelling are required to confirm the existence of radiation belts and possible plasma source in this and other brown dwarf systems.

Pooling data from all of the known ECM-emitting brown dwarfs and ultracool dwarfs demonstrates preliminary empirical evidence of a connection between their quiescent radio emission and auroral emission. Specifically, Pineda et al. (2017) show that Hα luminosities, one tracer of aurorae (Hallinan et al. 2015; Kao et al. 2016), correlate with quiescent radio luminosities for known M7–T6.5 auroral pulse emitters. The occurrence of quiescent radio emission also correlates with the occurrence of pulsed ECM aurorae. Only ∼5–10 per cent of dwarfs in each of the M, L, and T spectral types emit radio emission of any type (Route & Wolszczan 2016b). Of radio brown dwarfs, 15 of 24 (62 per cent) have been observed to emit at least one ECM pulse (Pineda et al. 2017). These correlations suggest that physical processes contributing to the quiescent radio emission and auroral emission of brown dwarfs and ultracool dwarfs may be related, as is the case for Jupiter.

Even in the event that quiescent brown dwarf radio emission is not related to their ECM emission, the high occurrence rate of pulsed radio emission amongst brown dwarfs and ultracool dwarfs with quiescent radio emission suggests that a preliminary search targeting quiescent emission still presents an efficient means for identifying ECM-emitting Y dwarf candidates.

4 CALIBRATIONS

We calibrated our measurement sets using the standard VLA flux calibrator 3C286, and nearby phase calibrators. Typical full-bandwidth sensitivity at BnA configuration for 3.5 h on source in *C*-band is 1.8 μJy and for C configuration on source in *C*-band for

Table 3. Summary of archival measurements sets for J1419+5423.

Project #	Obs. date	Block ID	Flux calibrator	Flux (Jy)
15A–102	2015 Feb 08	30105159	3C286	1.17593 ± 0.000058
14A–483	2014 Aug 10	29584695	3C286	1.3839 ± 0.0013
14A–483	2014 Sep 03	29606143	3C286	1.3968 ± 0.0013

1.5 h is 2.7 μJy with typical 3-bit observations reaching an absolute flux calibration accuracy of ∼5 per cent. Flux calibration accuracy may be reduced and result in systematically offset flux densities when gain calibrations interpolated from the phase calibrator are not sufficient to correct for the variation of gain phases with time. To account for this, our observations alternated between a nearby phase calibrator and the target source with typical integration times of 2 and 20 min, respectively. We obtained gain solutions for the phase calibrators that varied slowly and smoothly over time, suggesting that this source of error is negligible.

The main objective of our observations was to search for the presence of quiescent radio emission in our targets, so we did not observe polarization calibrators. Some flux can leak between the right and left polarizations at a level of 2–3 per cent, which can be mitigated with polarization calibrations to less than 0.5 per cent. For our objects and the sensitivity that we are achieving, this represents less than 0.1–0.2 μJy, which is more than an order of magnitude less than the rms noise.

We initially processed each measurement set with the VLA CASA 4.7.0 Calibration Pipeline, after which we flagged all remaining RFI and manually recalibrated as needed. As a rule, all data between 4.0–4.4 GHz was discarded due to extremely bright and persistent RFI. We obtained absolute flux by bootstrapping flux densities with the observed flux calibrators.

For *WISE* 0855−07, a nearby bright quasar with flux density ∼0.3 Jy limited initial rms sensitivity for the full measurement set to 153 μJy. After self-calibrating, rms sensitivity increased to 7.2 μJy, for a dynamic range exceeding 10^5. However, residual sidelobes remain in Stokes I. Additionally, there is sidelobe structure in Stokes V, which is a consequence of the brightness of the background source and the lack of polarization calibrations.

Similarly for *WISE* 1738+27, a nearby bright object with flux density ∼18 mJy limited initial sensitivity to 5.1 μJy. After self-calibrating, sensitivity increased to 3.2 μJy. For *WISE* 1405+55 we kept initial flags from the calibration pipeline before proceeding with a manual calibration.

Flux calibrator 3C295 was observed for *WISE* 1405+55, but it was fully resolved and could not be used to satisfactorily flux calibrate. Instead, we located the measurement set nearest in time to our observations in the VLA archive containing observations of the same phase calibrator that we used, quasar J1419+5423. These observations were taken on 2015 February 08 in B configuration at *C*-band using 3C286 as a flux calibrator. The emission from 3C286 is stable within 1 per cent over 30 yr for *C*-band (Perley & Butler 2013). After flux calibrating J1419+5423 with 3C286 in this archived measurement set, we transferred the flux calibrations to the phase calibrator field in our own measurement set, from which we then determined bandpass solutions. To check for time variability in the flux density of J1419+5423, we also calibrated two other archival measurement sets from 2014 August 10 and 2014 September 03 containing observations of J1419+5423 at *C*-band in D configuration. Measurements of the J1419+5423 flux densities in all epochs are listed in Table 3. Based on the above ∼month time-scales, we expect the measured flux of J1419+5423 and therefore *WISE* 1405+55 to be accurate within ∼20 per cent.

Table 4. Summary of archival measurements sets for J1419+5423.

Object	3σ Upper limit Stokes I, V (μJy)	1σ Upper limit (30 s) rr, ll (μJy)	Pulse (#)
WISE 0855−07	<21.6, <7.2	46.2, 46.0	0
WISE 1405+55	<6.6, <6.9	55.9, 51.3	0
WISE 1738+27	<9.6 < 8.7	34.3, 46.4	0

5 ANALYSIS AND RESULTS

We produced Stokes I and Stokes V (total and circularly polarized intensities, respectively) images for the entire observing block of each object with the CASA `clean` routine, modeling the sky emission frequency dependence with two terms and using natural weighting. We searched for a point source at the proper motion-corrected coordinates of each target. We fitted an elliptical Gaussian point source to the cleaned image of each object at its predicted coordinates using the CASA task `imfit`, but did not measure statistically significant flux densities. An examination by eye confirms the lack of a point source. Table 4 gives the 3σ upper limits on the flux density for each source. We did not detect any radio emission from any Y dwarf in the images, down to rms noise levels of 2.2 μJy for *WISE* 1405+55, 3.2 μJy *WISE* 1738+27, and 7.2 μJy for *WISE* 0855−07.

We searched the right- and left-circularly polarized (rr- and ll-correlations) timeseries of our targets for candidates of highly circularly polarized pulses that may have coincided with our observing blocks. To do this, we added phase delays to our visibility data to centre the expected locations of our targets at the phase centre using the CASA `fixvis` and followed the procedure outlined in section 4.2 of Kao et al. (2018) for 4–8 GHz, 4–6 GHz, and 6–8 GHz subbands. Fig. 1 shows the 4–8 GHz timeseries for each object and the rms noise for the timeseries is reported in Table 4.

The timeseries for *WISE* 0855−07 initially showed a possible pulse in both the rr and ll correlations at a UT time stamp of 24.7 h on 2015 May 21. Imaging at this time stamp showed that a residual sidelobe overlapped the target's expected coordinates and ruled out a pulse. We removed this sidelobe in our timeseries data and repeated the timeseries search procedure, which yielded no pulse candidates. We did not detect any circularly polarized radio pulses for either *WISE* 1405+55 or *WISE* 1738+27.

6 DISCUSSION

Despite the decreased sensitivity in the Stokes I imaging for *WISE* 0855−07, the proximity of our targets allows us to place stringent constraints on their radio luminosities. We compare the 3σ upper limits to quiescent emission flux densities observed for other radio brown dwarfs in Fig. 2. These upper limits are consistent with a tentative trend that cooler objects tend to be less radio bright in quiescent emission than warmer ultracool dwarfs (Pineda et al. 2017), but the data do not provide sufficient evidence for or against a break in this trend. We note that Route & Wolszczan (2016b) found tentative evidence of a decline in quiescent radio luminosities between spectral types L2 and T3. Two objects beyond spectral type T3 cause this tentative declining trend to appear to invert for very cold objects and are indicative of scatter. The lack of detectable Y

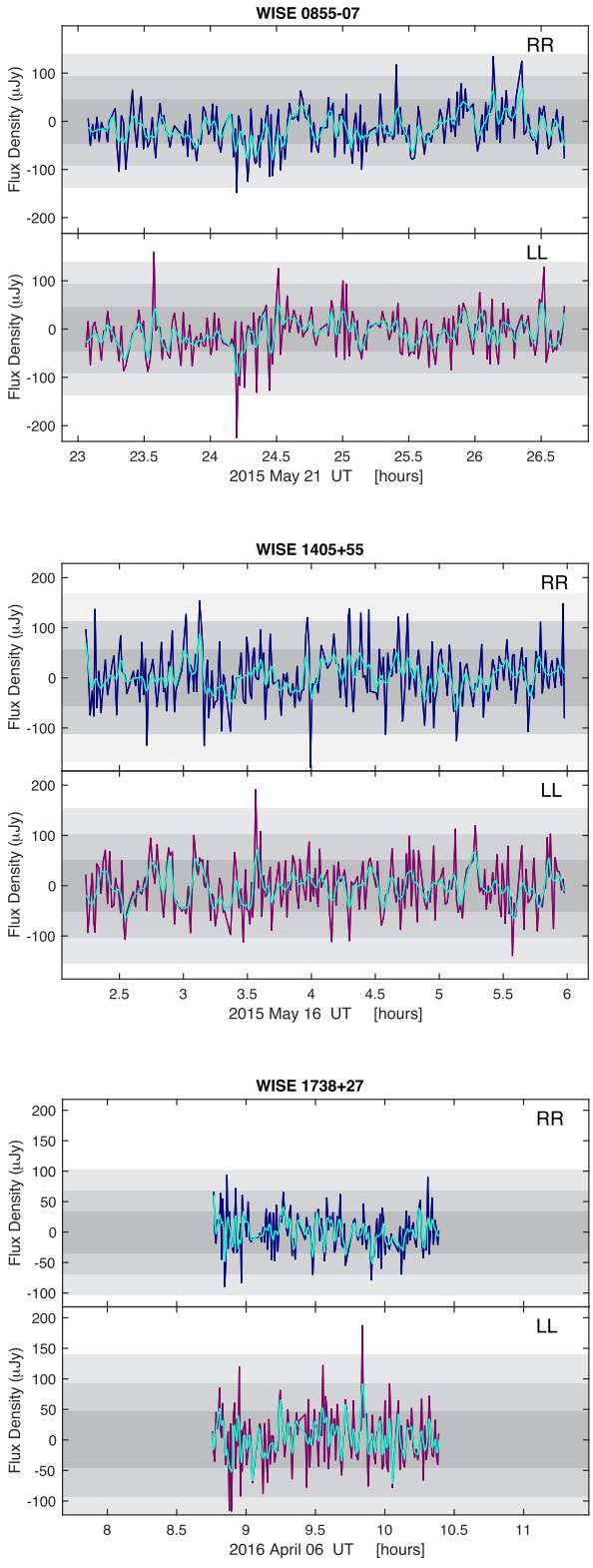

Figure 1. Timeseries of rr- and ll-correlated (blue and red, respectively) flux densities averaged over 30 s intervals. Grey regions indicate 1, 2, and 3σ rms noise. Cyan lines are smoothed timeseries used for identifying pulse candidates. No pulses are detected.

dwarf quiescent emission in our study here additionally highlights potential scatter in the observed quiescent luminosities and also the need for additional data in the T and Y spectral ranges to firmly establish any trend.

The upper limits on quiescent radio emission that we were able to place on *WISE* 1405+55 and *WISE* 1738+27 rule out quiescent emission at luminosities comparable to the faintest quiescent emission that was previously observed on earlier type cool dwarfs (see Fig. 2). For *WISE* 0855−07, the rms noise that we achieved in our images is not enough to rule out the possibility of quiescent emission at the tens of μJy level. However, because of its proximity, any quiescent radio luminosity would be an order of magnitude lower than what has previously been observed in any M7 or later dwarf. If the quiescent emission is not strongly variable at these frequencies for Y dwarfs, quiescent emission in *WISE* 0855−07 may be unlikely.

The Jovian radiation belts tap rotational energy to accelerate trapped electrons to mildly relativistic energies as in Jupiter (Horne et al. 2008). If brown dwarf quiescent emission also originates from radiation belts, then insufficient rotational energy may preclude the formation of strong radiation belts around Y dwarfs. However, Y dwarf rotational speeds are not expected to depart dramatically from those of earlier type brown dwarfs. Cool Y dwarf atmospheres, even more so than the warmer M, L, and T dwarfs, limit the production of significant stellar winds and likely allow these objects to sustain fast rotation periods, on the order of several hours, for much of their lifetimes (e.g. Pineda et al. 2017). Additionally, as brown dwarfs cool with age they also contract. This effect may also help maintain rapid rotation rates in the Y dwarf population. The field population of brown dwarfs shows a peak in its rotation period distribution at less than 5 h (Radigan et al. 2014), and Y dwarf periods are likely similar, suggesting that they may have sufficient rotational energy to power radiation belt electron populations.

6.1 Magnetic field implications

Future studies demonstrating a systematic absence of detectable radio emission at these frequencies may be evidence for a dynamo branch occupied by M, L, and T dwarfs that is distinct from a branch occupied by Y dwarfs and their planetary cousins. Viewing geometries do not strongly affect the detectability of ECM emission (Pineda et al. 2017), so a systemic lack of GHz ECM emission from Y dwarfs could be attributable to a corresponding lack of kilogauss fields. If quiescent emission in brown dwarfs proves to be attributable to radiation belts, then such a systemic lack of quiescent emission could point to the onset of large-scale fields that cannot capture particles at a similar efficiency as in M, L, and T dwarfs. Such a scenario would be analogous to the weak radiation belts observed on Uranus and Neptune, which have smaller magnetospheres that are not dominated by dipoles (Schubert & Soderlund 2011). These smaller magnetospheres may be less efficient at accelerating trapped electrons and/or at capturing particles than the dipole-dominated fields of Earth, Jupiter, and Saturn (Kivelson 2007, and references therein). Alternatively, they may have rings that absorb radiation belt particles, such as for Saturn (Mauk & Fox 2010).

A detection of pulsed, circularly polarized radio emission from any of these Y dwarfs would have indicated the presence of large-scale magnetic fields of at least 1.6 kG. In the absence of any detectable ECM emission from our targets, we cannot conclusively

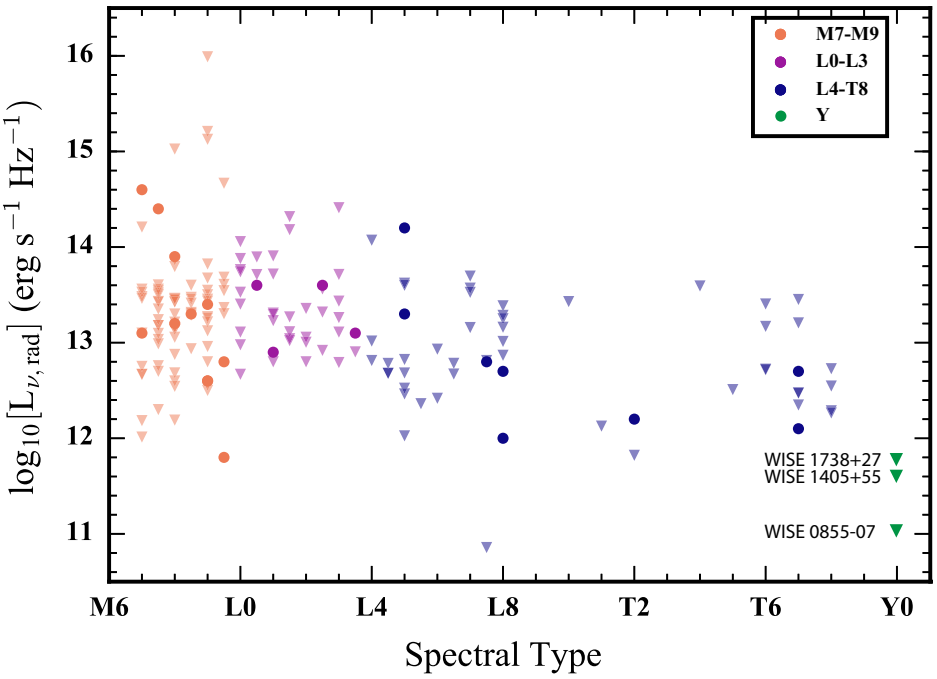

Figure 2. Quiescent emission radio luminosities as a function of spectral type. Upper limits are triangles and detections are circles. Adapted from Figure 7 of Pineda et al. (2017) and reproduced by permission of the American Astronomical Society.

provide any strong constraints on magnetic field strengths in any of our targets. Below, we explore why.

The premise of our observing strategy is a possible link between the quiescent and ECM radio emission observed on other brown dwarfs. If quiescent radio emission is indeed linked to pulsed radio emission, for instance in the manner that we discuss in Section 3.1, then the lack of pulse detections would be expected given the lack of detectable quiescent emission. If quiescent emission is not linked to ECM emission, then the lack of detections of ECM pulses may be because our observations do not span the entire rotational periods of our targets. Additionally, the following possibilities may be the case: (1) our targets may have strong fields but do not produce detectable auroral radio emission and (2) currents powering auroral activity in these Y dwarfs are variable in nature.

In case (1), ECM emission will not occur if the engine for driving such emission is not present, despite the presence of sufficiently strong fields. In fact, Zeeman broadening measurements confirm mean surface field strengths in M7–M9 dwarfs that are strong enough to drive ECM emission at several GHz (Morin et al. 2010; Reiners & Basri 2010; Berdyugina et al. 2017; Shulyak et al. 2017), yet not all of these strongly magnetized ultracool dwarfs have been detected in radio (e.g. Antonova et al. 2013; Route & Wolszczan 2013; Williams et al. 2014; Lynch et al. 2016; Route & Wolszczan 2016b; Guirado et al. 2018, and references therein). While possible mechanisms for generating aurorae in brown dwarfs remain unconfirmed, if the primary driver for ECM emission in isolated brown dwarfs is co-rotation breakdown of a plasma sheet in the magnetosphere (and references therein Cowley & Bunce 2001; Hill 2001; Bagenal et al. 2014; Badman et al. 2015), slower rotation may prevent such co-rotation breakdown from occurring (Nichols et al. 2012).

Indeed, Pineda et al. (2017) indicate that several conditions are required to generate significant auroral emission, regardless of the underlying engine, including at least rapid rotation and strong magnetic field strengths. Esplin et al. (2016) and Cushing et al. (2016) have reported rotational periods derived from infrared variability at 8.5 h for *WISE* 0855−07, 5.3–9.3 h for *WISE* 1405+55, and 3.0–6.0 h for *WISE* 1738+27. In comparison, all pulsing radio brown dwarfs have reported rotational periods between 1.77 and 3.89 h (Pineda et al. 2017; Kao et al. 2018, and references therein). In contrast, Jupiter and Saturn, with mean dipole fields between 2–3 orders of magnitude weaker than kilogauss brown dwarf mean fields, both have rotation periods between ∼10–10.75 h (Zarka 1998), and co-rotation breakdown powers the main auroral oval in Jupiter and dominates the Saturnian aurora (Cowley & Bunce 2001; Mauk & Bagenal 2012). Given the longer reported rotational velocities for our targets, it is possible that the magnetic fields of our targets may be sufficiently strong to suppress co-rotation breakdown, especially for *WISE* 0855−07. If the true rotational period of *WISE* 1738+27 is in the low end of its reported range, then it may lack other necessary ingredients for large-scale auroral current systems.

In case (2), necessary conditions for the occurrence of large-scale auroral current systems include (a) the presence of mildly relativistic populations of free electrons within the large-scale magnetospheres of our objects, (b) the presence of strong, large-scale magnetic fields, and (c) the presence of a satellite magnetosphere or ionosphere for aurora generated by satellite-interactions. Even in the case that our targets have strong magnetic fields, aurora will not occur if conditions (a) and (c) are not met, and all three conditions provide opportunities for time-varying auroral emission.

With regards to condition (a), sufficiently intermittent periods of volcanic activity from a satellite may cause time varying auroral activity. In the Jupiter system, vigorous volcanic activity from Io replenishes the plasma torus on a time-scale of ∼19 d, and its density, temperature, and composition can vary up to a factor of two (Delamere & Bagenal 2003). Long-term monitoring show that the brightness of Jovian auroral satellite footprints (Io, Ganymede)

can vary by a factor of ∼2–10, and the brightest emission coincides with when the satellites approach the centre of the plasma torus, where denser plasma is expected to generate a stronger interaction (GéRard et al. 2006; Serio & Clarke 2008; Grodent et al. 2009; Wannawichian, Clarke & Nichols 2010). For condition (b), a magnetic cycle in which large-scale fields evolve into small-scale fields may cause time variation in auroral activity (e.g. Kitchatinov, Moss & Sokoloff 2014; Route 2016; Yadav et al. 2016). For condition (c), the transient ionosphere of Enceladus provides a model for producing time-varying auroral emission. Enceladus can (rarely) generate a detectable auroral footprint with high-amplitude variability (factor of ∼3) over a time-scale of a few hours, which is attributed to its time-variable cryo-volcanism (Pryor et al. 2011). Alternatively, a satellite undergoing its own magnetic cycling could also cause an intermittent analogue of the Jupiter-Io current system. We note that this last example is purely speculative and has not yet been observed.

While the data preclude concrete conclusions about magnetic field strengths and auroral generation mechanisms in Y dwarfs, longer term monitoring is necessary to resolve the possibilities discussed in case (2). For case (1), a broader sample of cool dwarfs spanning a range of masses and rotation rates will provide insight into whether there are any associated dependencies for either. Given that all known radio pulsing brown dwarfs are fast rotators, an initial focus on Y dwarfs with short rotation periods would be especially compelling.

Finally, it is certainly possible the that quiescent emission and any potential ECM emission observed in Y dwarfs is not in fact linked. If future campaigns reveal no detectable quiescent emission in Y dwarfs, this hypothesis could be tested with observations of all known Y dwarfs with time blocks spanning the entire rotation period of each target.

7 CONCLUSIONS

We have postulated that brown dwarf pulsing radio emission, attributed to the electron cyclotron maser mechanism, may be related to non-bursting quiescent radio emission. We presented a possible paradigm to describe previously observed correlations between brown dwarf quiescent and ECM radio emission, quiescent radio and Hα luminosities of known brown dwarf auroral emitters, and infrared variability with the occurrence rate of ECM radio emission in brown dwarfs.

Using this paradigm, we have observed three Y dwarfs known to display evidence of infrared variability for radio emission that may select for auroral magnetospheric currents. In the interest of conserving limited telescope time resources, we elected to initially search for quiescent radio emission as a proxy for pulsed emission, aiming to follow up any quiescent detections with a comprehensive search for pulsed emission. We did not detect any radio emission and cannot conclusively provide meaningful constraints on Y dwarf magnetism. Instead, follow-up observations of these initially quiet targets will be key for ruling out time variability in auroral current systems.

The limiting factor for Y dwarf radio detections is not sensitivity but rather the number of sources observed. Detection fractions for M, L, and T dwarfs are approximately constant at ∼5–10 per cent for each spectral type (Route & Wolszczan 2016b), and this detection fraction may extend to early Y dwarfs as well. True fractions are likely higher, since these include surveys prior to the upgraded VLA and with Arecibo, which is insensitive to quiescent emission (and references therein Route & Wolszczan 2016b; Pineda et al. 2017). While quiescent radio luminosities may depend weakly on spectral type (Route & Wolszczan 2016b; Pineda et al. 2017), selection effects bias the known Y dwarf population to be very nearby and exposure times can be adjusted to further mitigate sensitivity concerns. Future surveys will require a combination of more objects and deeper observations to provide meaningful constraints on Y dwarfs magnetic fields.

ACKNOWLEDGEMENTS

The National Radio Astronomy Observatory is a facility of the National Science Foundation operated under cooperative agreement by Associated Universities, Inc. Support for this work was provided by the National Science Foundation (NSF) through the Grote Reber Fellowship Program administered by Associated Universities, Inc./National Radio Astronomy Observatory; by a grant from the NSF Graduate Research Fellowship under Grant DGE-1144469; and by the NSF Grant AST-1654815. Support for this work was provided by the National Aeronautics and Space Administration (NASA) through the NASA Hubble Fellowship grant #HST-HF2-51411.001-A awarded by the Space Telescope Science Institute, which is operated by the Association of Universities for Research in Astronomy, Inc., for NASA, under contract NAS5-26555.

REFERENCES

André N. et al., 2008, Rev. Geophys., 46, RG4008
Antonova A., Doyle J. G., Hallinan G., Golden A., Koen C., 2007, A&A, 472, 257
Antonova A., Hallinan G., Doyle J. G., Yu S., Kuznetsov A., Metodieva Y., Golden A., Cruz K. L., 2013, A&A, 549, 14
Apai D., Radigan J., Buenzli E., Burrows A., Reid I. N., Jayawardhana R., 2013, ApJ, 768, 121
Badman S. V., Branduardi-Raymont G., Galand M., Hess S. L. G., Krupp N., Lamy L., Melin H., Tao C., 2015, Space Sci. Rev., 187, 99
Bagenal F. et al., 2014, Space Sci. Rev., 1
Basharinov A. E., Gurvich A. S., Egorov S. T., 1974, Moscow Izdatel Nauka, p. 188
Beichman C., Gelino C. R., Kirkpatrick J. D., Cushing M. C., Dodson-Robinson S., Marley M. S., Morley C. V., Wright E. L., 2014, ApJ, 783, 68
Berdyugina S. V., Solanki S. K., 2002, A&A, 385, 701
Berdyugina S. V., Harrington D. M., Kuzmychov O., Kuhn J. R., Hallinan G., Kowalski A. F., Hawley S. L., 2017, ApJ, 847, 61
Berger E. et al., 2001, Nature, 410, 338
Berger E. et al., 2009, ApJ, 695, 310
Berger E. et al., 2010, ApJ, 709, 332
Berger E., 2002, ApJ, 572, 503
Berger E., 2006, ApJ, 648, 629
Bhardwaj A., Gladstone G. R., 2000, Rev. Geophys., 38, 295
Bolton S. J., Thorne R. M., Bourdarie S., de Pater I., Mauk B., 2004, Jupiter's inner radiation belts. Cambridge Univ. Press, Cambridge, p. 671
Bower G. C., Loinard L., Dzib S., Galli P. A. B., Ortiz-León G. N., Moutou C., Donati J.-F., 2016, ApJ, 830, 107
Brice N., Mcdonough T. R., 1973, Icarus, 18, 206
Browning M. K., 2008, ApJ, 676, 1262
Burgasser A. J. et al., 2014, ApJ, 785, 10
Burgasser A. J., Putman M. E., 2005, ApJ, 626, 486
Burgasser A. J., Melis C., Zauderer B. A., Berger E., 2013, ApJ, 762, L3
Burgasser A. J., Melis C., Todd J., Gelino C. R., Hallinan G., Bardalez Gagliuffi D., 2015, AJ, 150, 180
Christensen U. R., Aubert J., 2006, Geophys. J. Int., 166, 97
Christensen U. R., Holzwarth V., Reiners A., 2009, Nature, 457, 167

Clarke J. T., Grodent D., Cowley S. W. H., Bunce E. J., Zarka P., Connerney J. E. P., Satoh T., 2004, in Bagenal F., Dowling T. E., McKinnon W. B., eds, Jupiter's aurora. Cambridge Univ. Press, Cambridge, p. 639
Cowley S. W. H., Bunce E. J., 2001, Planet. Space Sci., 49, 1067
Kirk R. L., Soderblom L. A., Brown R. H., Kieffer S. W., Kargel J. S., 1995, in Cruikshank D. P., Matthews M. S., Schumann A. M., eds, Neptune and Triton. Univ. Arizona Press, Tuscon, p. 949
Cushing M. C. et al., 2011, ApJ, 743, 17
Cushing M. C. et al., 2016, ApJ, 823, 11
de Pater I., Sault R. J., Butler B., DeBoer D., Wong M. H., 2016, Science, 352, 1198
Delamere P. A., Bagenal F., 2003, J. Geophys. Res.: Space Phys., 108, 1276
Donati J.-F., Forveille T., Collier Cameron A., Barnes J. R., Delfosse X., Jardine M. M., Valenti J. A., 2006, Science, 311, 633
Dupuy T. J., Kraus A. L., 2013, Science, 341, 1492
Dyudina U. A., Ingersoll A. P., Ewald S. P., Wellington D., 2016, Icarus, 263, 32
Esplin T. L., Luhman K. L., Cushing M. C., Hardegree-Ullman K. K., Trucks J. L., Burgasser A. J., Schneider A. C., 2016, ApJ, 832, 58
Faherty J. K., Tinney C. G., Skemer A., Monson A. J., 2014, ApJ, 793, L16
Gallagher D. L., Dangelo N., 1981, Geophys. Res. Lett., 8, 1087
Ganushkina N. Y., Dandouras I., Shprits Y. Y., Cao J., 2011, J. Geophys. Res.: Space Phys., 116, A09234
Gastine T., Morin J., Duarte L., Reiners A., Christensen U. R., Wicht J., 2013, A&A, 549, 4
Gawroński M. P., Goździewski K., Katarzyński K., 2017, MNRAS, 466, 4211
GéRard J.-C., Saglam A., Grodent D., Clarke J. T., 2006, J. Geophys. Res.: Space Phys. 111, A04202
Girard J. N. et al., 2016, A&A, 587, A3
Gizis J. E., Monet D. G., Reid I. N., Kirkpatrick J. D., Liebert J., Williams R. J., 2000, AJ, 120, 1085
Grodent D., Bonfond B., Radioti A., Gérard J.-C., Jia X., Nichols J. D., Clarke J. T., 2009, J. Geophy. Res.: Space Phys., 114, A07212
Guirado J. C., Azulay R., Gauza B., Pérez-Torres M. A., Rebolo R., Climent J. B., Zapatero Osorio M. R., 2018, A&A, 610, 6
Gurnett D. A. et al., 2002, Nature, 415, 985
Hallinan G. et al., 2007, ApJ, 663, L25
Hallinan G. et al., 2015, Nature, 523, 568
Hallinan G., Antonova A., Doyle J. G., Bourke S., Brisken W. F., Golden A., 2006, ApJ, 653, 690
Hallinan G., Antonova A., Doyle J. G., Bourke S., Lane C., Golden A., 2008, ApJ, 684, 644
Hallinan G., Sirothia S. K., Antonova A., Ishwara-Chandra C. H., Bourke S., Doyle J. G., Hartman J., Golden A., 2013, ApJ, 762, 34
Harding L. K., Hallinan G., Boyle R. P., Golden A., Singh N., Sheehan B., Zavala R. T., Butler R. F., 2013, ApJ, 779, 101
He M. Y., Triaud A. H. M. J., Gillon M., 2017, MNRAS, 464, 2687
Hill T. W., 2001, J. Geophys. Res., 106, 8101
Horne R. B., Thorne R. M., Glauert S. A., Douglas Menietti J., Shprits Y. Y., Gurnett D. A., 2008, Nature Phys., 4, 301
Hudson M. K., Kress B. T., Mazur J. E., Perry K. L., Slocum P. L., 2004, J. Atmos. Sol.-Terr. Phys., 66, 1389
Hudson M. K., Kress B. T., Mueller H.-R., Zastrow J. A., Bernard Blake J., 2008, J. Atmos. Sol.-Terr. Phys., 70, 708
Johns-Krull C. M., Valenti J. A., 1996, ApJ, 459, L95
Kao M. M., Hallinan G., Pineda J. S., Escala I., Burgasser A., Bourke S., Stevenson D., 2016, ApJ, 818, 24
Kao M. M., Hallinan G., Pineda J. S., Stevenson D., Burgasser A., 2018, ApJS, 237, 25
Kellermann K. I., 1970, Radio Sci., 5, 487
Khurana K. K., Kivelson M. G., Vasyliunas V. M., Krupp N., Woch J., Lagg A., Mauk B. H., Kurth W. S., 2004, in Bagenal F., Dowling T. E., McKinnon W. B., eds, The configuration of Jupiter's magnetosphere. Cambridge Univ. Press, Cambridge, p. 593
Kirkpatrick J. D. et al., 2011, ApJS, 197, 55
Kirkpatrick J. D. et al., 2012, ApJ, 753, 38
Kitchatinov L. L., Moss D., Sokoloff D., 2014, MNRAS, 442, L1
Kivelson M. G., 2007, in Kamide Y., Chian C.-L., eds, Planetary Magnetospheres. Springer-Verlag, New York, p. 470
Kloosterman J. L., Butler B., de Pater I., 2008, Icarus, 193, 644
Leggett S. K. et al., 2016, ApJ, 830, 9
Luhman K. L., 2014, ApJ, 786, L18
Luhman K. L., Esplin T. L., 2016, AJ, 152, 78
Lynch C., Mutel R. L., Güdel M., 2015, ApJ, 802, 106
Lynch C., Murphy T., Ravi V., Hobbs G., Lo K., Ward C., 2016, MNRAS, 457, 1224
Lynch C. R., Murphy T., Kaplan D. L., Ireland M., Bell M. E., 2017, MNRAS, 467, 3447
Maillard J., Miller S., 2011, in Beaulieu J. P., Dieters S., Tinetti G., eds, ASP Conf. Ser. Vol. 450, Molecules in the Atmospheres of Extrasolar Planets. Astron. Soc. Pac., San Francisco, p. 19
Marley M. S., Saumon D., Goldblatt C., 2010, ApJ, 723, L117
Mauk B., Bagenal F., 2012, Washington DC American Geophysical Union Geophysical Monograph Series, vol. 197. American Geophysical Union, Washington, DC
Mauk B. H., Fox N. J., 2010, J. Geophys. Res.: Space Phys., 115, A12220
McLean M., Berger E., Irwin J., Forbrich J., Reiners A., 2011, ApJ, 741, 27
McLean M., Berger E., Reiners A., 2012, ApJ, 746, 23
Metchev S. A. et al., 2015, ApJ, 799, 23
Miles-Páez P. A., Metchev S. A., Heinze A., Apai D., 2017, ApJ, 840, 83
Mohanty S., Basri G., Shu F., Allard F., Chabrier G., 2002, ApJ, 571, 469
Moore L. et al., 2017, Geophys. Res. Lett., 44, 4513
Morin J., Donati J.-F., Petit P., Delfosse X., Forveille T., Jardine M. M., 2010, MNRAS, 407, 2269
Morin J., Dormy E., Schrinner M., Donati J.-F., 2011, MNRAS, 418, L133
Morley C. V., Marley M. S., Fortney J. J., Lupu R., 2014, ApJ, 789, L14
Murphy T. et al., 2015, MNRAS, 446, 2560
Mutel R. L., Menietti J. D., Christopher I. W., Gurnett D. A., Cook J. M., 2006, J. Geophys. Res.: Space Phys., 111, A10203
Nichols J. D., Burleigh M. R., Casewell S. L., Cowley S. W. H., Wynn G. A., Clarke J. T., West A. A., 2012, ApJ, 760, 59
Parker E. N., 1975, ApJ, 198, 205
Perley R. A., Butler B. J., 2013, ApJS, 204, 19
Phan-Bao N., Osten R. A., Lim J., Martin E. L., Ho P. T. P., 2007, ApJ, 658, 553
Pineda J. S., 2016, PhD thesis, California Institute of Technology
Pineda J. S., Hallinan G., Kao M. M., 2017, ApJ, 846, 75
Pryor W. R. et al., 2011, Nature, 472, 331
Radigan J., Lafrenière D., Jayawardhana R., Artigau E., 2014, ApJ, 793, 75
Rajan A. et al., 2015, MNRAS, 448, 3775
Reiners A., 2012, Liv. Rev. Sol. Phys., 9, 1
Reiners A., Basri G., 2006, ApJ, 644, 497
Reiners A., Basri G., 2007, ApJ, 656, 1121
Reiners A., Basri G., 2008, ApJ, 684, 1390
Reiners A., Basri G., 2009, A&A, 496, 787
Reiners A., Basri G., 2010, ApJ, 710, 924
Rodríguez-Barrera M. I., Helling C., Stark C. R., Rice A. M., 2015, MNRAS, 454, 3977
Route M., 2016, ApJ, 830, 5
Route M., 2017, ApJ, 845, 66
Route M., Wolszczan A., 2012, ApJ, 747, L22
Route M., Wolszczan A., 2013, ApJ, 773, 18
Route M., Wolszczan A., 2016a, ApJ, 821, L21
Route M., Wolszczan A., 2016b, ApJ, 830, 85
Saar S. H., 1994, in Rabin D. M., Jefferies J. T., Lindsey C., eds, IAU Symp. 154, Infrared Solar Physics. Kluwer, Dordrecht, p. 437
Schmidt S. J., Hawley S. L., West A. A., Bochanski J. J., Davenport J. R. A., Ge J., Schneider D. P., 2015, AJ, 149, 158
Schneider A. C. et al., 2015, ApJ, 804, 17
Schrijver C. J., 2009, ApJ, 699, L148
Schubert G., Soderlund K. M., 2011, Phys. Earth Planet. Inter., 187, 92
Serio A. W., Clarke J. T., 2008, Icarus, 197, 368
Shulyak D., Reiners A., Wende S., Kochukhov O., Piskunov N., Seifahrt A., 2010, A&A, 523, 12

Shulyak D., Reiners A., Engeln A., Malo L., Yadav R., Morin J., Kochukhov O., 2017, Nature Astron., 1, 0184
Simitev R. D., Busse F. H., 2009, Europhys. Lett., 85, 5
Skemer A. J. et al., 2016, ApJ, 826, 5
Stansberry K. G., White R. S., 1974, J. Geophys. Res., 79, 2331
Stone E. C., Miner E. D., 1986, Science, 233, 39
Treumann R. A., 2006, A&AR, 13, 229
Turnpenney S., Nichols J. D., Wynn G. A., Casewell S. L., 2017, MNRAS, 470, 4274
Valenti J. A., Marcy G. W., Basri G., 1995, ApJ, 439, 939
Walt M., 2005, Introduction to Geomagnetically Trapped Radiation. Cambridge Univ. Press, Cambridge
Wannawichian S., Clarke J. T., Nichols J. D., 2010, J. Geophys. Res.: Space Phys., 115, A02206
West A. A., Hawley S. L., Bochanski J. J., Covey K. R., Reid I. N., Dhital S., Hilton E. J., Masuda M., 2008, AJ, 135, 785
Williams P. K. G., Berger E., 2015, ApJ, 808, 189
Williams P. K. G., Berger E., Zauderer B. A., 2013, ApJ, 767, L30
Williams P. K. G., Cook B. A., Berger E., 2014, ApJ, 785, 9
Williams P. K. G., Casewell S. L., Stark C. R., Littlefair S. P., Helling C., Berger E., 2015, ApJ, 815, 64
Williams P. K. G., Gizis J. E., Berger E., 2017, ApJ, 834, 117
Winglee R. M., 1985, J. Geophys. Res., 90, 9663
Wright E. L. et al., 2010, AJ, 140, 1868
Yadav R. K., Christensen U. R., Wolk S. J., Poppenhaeger K., 2016, ApJ, 833, L28
Zarka P., 1998, J. Geophys. Res., 103, 20159
Zarka P., 2007, Planet. Space Sci., 55, 598

This paper has been typeset from a TEX/LATEX file prepared by the author.